

Effects of Ti addition on LFZ Bi-2212 thin rods

L.A. ANGUREL ^a, M. MORA ^a, J.C. DÍEZ ^a, R.J. DROST ^b, P.H. KES ^b

^a Dpto. de Ciencia y Tecnología de Materiales y Fluidos, Inst. Ciencia de Materiales de Aragón (C.S.I.C.-Universidad de Zaragoza) Zaragoza, Spain

^b Kamerlingh Onnes Laboratory, Leiden University. 2333 CA Leiden, The Netherlands

In order to reproduce previous results in Bi-2212 single crystals, the effects associated with the addition of Ti to the precursors of Laser Floating Zone textured Bi-2212 thin rods have been analyzed. It has been found that Ti induces a great number of nucleation centers in the molten zone and, in consequence, it reduces the grain size one order of magnitude. In addition, using the same growth conditions, the texture of the sample is strongly degraded. These microstructural changes strongly affect the superconducting properties showing that Ti addition destroys the network of low angle grain boundaries that are responsible for the high critical currents in these materials.

Keywords: Superconductors, Ti doping, Laser Floating Zone Melting

Efecto de la introducción de Ti en barras bi-2212 texturadas mediante LFZ

Se ha analizado el efecto de la introducción de Ti en precursores de Bi-2212 para ser texturados mediante láser a través del método de zona flotante, todo ello debido a los resultados esperanzadores obtenidos en monocristales. Se ha encontrado que el Ti introduce un gran número de centros de nucleación en la zona fundida, por lo que se reducen las dimensiones de los granos en un orden de magnitud aproximadamente. Por otra parte, y utilizando las mismas condiciones de crecimiento, se observa que la textura de la muestra se degrada severamente. Estos cambios microestructurales afectan en gran medida a las propiedades superconductoras, demostrándose que la introducción de Ti destruye la red de fronteras de grano de bajo ángulo, que son las responsables en estos materiales de las altas corrientes críticas.

Palabras clave: Superconductores de alta temperatura, Ti dopaje, Fusión zonal flotante láser

1. INTRODUCTION

The development of hybrid current leads is one of the main technological applications of high temperature superconductors. In particular, in the near future, the development of cryocooler systems will extend the fields at which superconducting technology can be applied. In these equipments, hybrid current leads are absolutely necessary in order to minimize the heat load into the system. Bulk $\text{Bi}_2\text{Sr}_2\text{CaCu}_2\text{O}_{8+\delta}$ (Bi-2212) materials are good candidates for the superconducting part of the current lead because they combine high critical current densities (J_c) at low temperatures and a very low thermal conductivity (1). However, the high anisotropy and the short coherence length lead to the strong influence of thermal fluctuations at relatively high temperatures. This process limits the range of application of Bi-2212 compounds at high temperatures and high magnetic fields. Consequently, from a technological point of view, an improvement of flux pinning is desirable in order to extend the range of application of these materials.

One way to introduce new pinning centers is the use of texturing processes. It has previously been shown that the Laser Floating Zone melting technique (LFZ) (2) induces a textured microstructure in Bi-2212 compounds that creates strong intergranular pinning centers (3). The superconducting grains tend to form colonies with their a-b planes nearly parallel to the rod axis. These colonies form a network of low angle grain boundaries that have been considered as strong pinning centers. This fact can explain the shift of the irreversibility line to higher fields in comparison to single-

crystal samples and the high critical currents of the textured materials (4). It also follows from the presence of two peaks in the pinning energy distribution, one at low energies similar to that observed in single crystals, and another at high energies that has been correlated to intergranular effects (5).

In the case of intragranular pinning, best results in Bi-2212 single-crystals have been obtained by irradiation with heavy ions (6), neutrons (7) or protons (8) that introduces microscopic defects in the sample. Due to the low penetration of heavy ions in solids this technique is not adequate to be used in bulk materials. In addition, its cost makes it infeasible for technological applications. An alternative that has produced good results in Bi-2212 single-crystals is the chemical doping. In particular, doping of Ti (9, 10) or Pb (11) increases the pinning properties of these materials. In this case, the addition of Ti induces the presence of planar defects extended along the a-c plane. These defects form effective pinning centers when the field is applied along the c direction even if the critical temperature, T_c , is about 10 K lower than in undoped samples. Similar studies in polycrystalline samples show that Pb doping increases the intragranular pinning at temperatures higher than 40 K (12). However, for instance, doping of Ga does not improve the pinning of the composites (13).

In this paper we combine both methods, the Ti doping and the LFZ texturing process. We want to know the effect of Ti doping in the microstructure of the samples in order to know whether this addition modifies the intergranular pinning. We will also describe the influence of Ti addition on the superconducting properties of LFZ Bi-2212 textured samples.

2. EXPERIMENTAL

Two different precursors were prepared: one without Ti and one with an addition of 2 at% Ti. Powders of Bi_2O_3 , SrCO_3 , CaCO_3 , CuO and Ti were mixed in the ratios: Bi:Sr:Ca:Cu:Ti=2.0:1.9:1.0:(2.0-x):x ($x=0$ and $x=0.04$ (2 at% Ti)). After a drying procedure, the mixtures were calcined in air at 810°C . The resulting powders were pressed into cylinders of approximately 2 mm in diameter. These precursors were textured using a Nd:YAG ($\lambda=1064$ nm) laser beam split into three branches. The growth process was carried out with a rotation speed of 27 rpm and a growth rate of 30 mm/h. We will denote sample A the undoped one and sample B the sample with Ti. In addition, a doped sample has been grown at 60 mm/h (sample C).

The final textured samples had a diameter of 1.40-1.45 mm and a length of 5 cm. As-grown samples are not superconducting (14) and, in consequence, a further anneal treatment at 843°C in air has been given.

The microstructure of both as-grown and annealed samples has been studied by SEM analysis in a JEOL 600 microscope. The different phases that are present in the samples have been detected from EDX elemental analysis. The grain size distribution has been measured directly from digitized images using a standard image-processing program implemented by Link Analytical. From the size of the different grains, this program provides the average grain size and the standard deviation, σ_d .

AC susceptibility and magnetization measurements were carried out using a Quantum Design SQUID magnetometer. The superconducting transition has been determined from ac susceptibility measurements using an ac field applied parallel to the rod axis with amplitude of 0.2 Oe and a frequency of 171 Hz. Magnetization hysteresis loops were measured with the magnetic field applied parallel and perpendicular to the rod axis at temperatures between 5 and 25 K. Dc resistivity measurements were performed using a dc bias current of 1 mA. The I-V characteristics, in the temperature range 65-77 K, were obtained using sinusoidal current pulses with a period of 2 s.

3. MICROSTRUCTURE

3.1. Effect of Ti addition in the grain size distribution

Fig. 1a and 1b show a fractured cross-section of samples A and B. As it can be observed, the addition of Ti introduces two main differences in the microstructure of the textured samples. The first one is related with the grain size. As it can be observed in table I, where the average transverse grain size of the studied samples is presented, Ti addition strongly reduces their size. This observation reminds of the fact that Ti, as a pure element or as TiO_2 , is used as a heterogeneous nucleation agent in the processing of many materials as in HSLA steels (16) or in the controlled crystallization in glass-ceramics (17). Ti induces nucleation centers, reduces the initial grain size and allows controlling how they grow and, in consequence, the final properties of the materials.

In these Bi-2212 textured materials, the grains form platelet-like colonies with the c-axis perpendicular to the plane. In the undoped sample, the maximum in the thickness distribution appears at $6.5 \mu\text{m}$. By contrast, these values are reduced to

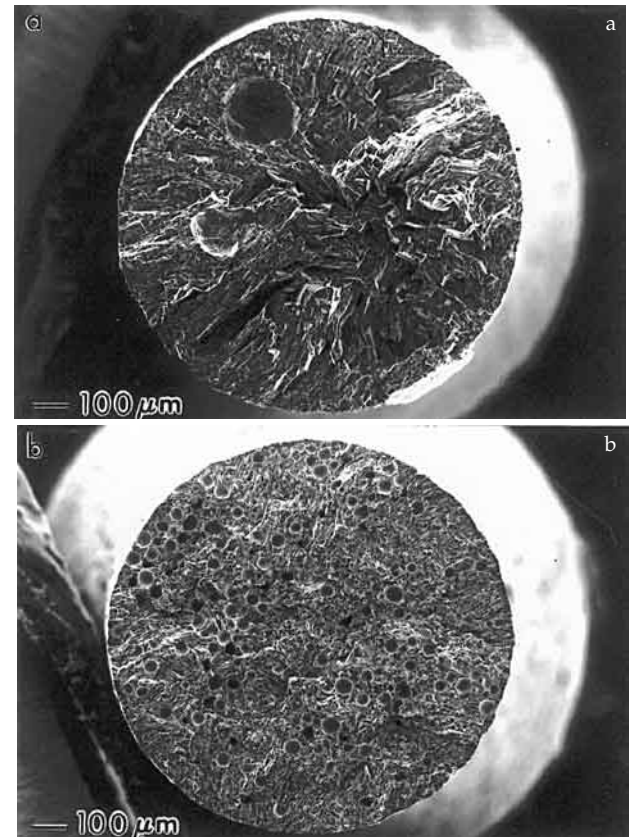


Fig. 1: Secondary electron micrographs of the transverse fractured sections for sample A (a) and sample B (b). The different bubbles that are present inside the samples can be observed in these full section micrographs.

TABLE I. TYPICAL VALUES OF THE TRANSVERSE COLONY SIZE DISTRIBUTION FOR THE STUDIED SAMPLES. THESE VALUES HAVE BEEN ESTIMATED FROM THE DIGITISED IMAGES.

	$\langle w \rangle$ (μm)	σ_d (μm)	$\langle c \rangle$ (μm)	σ_d (μm)
Sample A	37.0	19.9	6.5	2.4
Sample B	18.0	7.6	2.0	0.7
Sample C	10.4	4.3	1.1	0.6

$2.0 \mu\text{m}$ and $1.1 \mu\text{m}$ in the doped B and C samples, respectively. This influence of the growth rate was also measured in undoped samples, where an increase of the growth rate leads to a reduction of the grain size (14). A similar behavior has been observed in the evolution of the width of the colonies, the second dimension that can be measured in the transverse cross-section. It changes from values around $37.0 \mu\text{m}$ in sample A to $18.0 \mu\text{m}$ in B and $10.4 \mu\text{m}$ in sample C.

The second difference is related to the presence of bubbles in the samples. As it was previously observed in undoped samples (15), there are large bubbles with diameters of the order of $150\text{--}200 \mu\text{m}$ (Fig. 1a). They originate from the densification process that takes place during texturing and to the presence of carbonates in the precursors. In the doped sample, these bubbles are smaller, with diameters between 20 and $40 \mu\text{m}$, but they are more uniformly distributed all along the cross-section of the sample. This reduction could be related

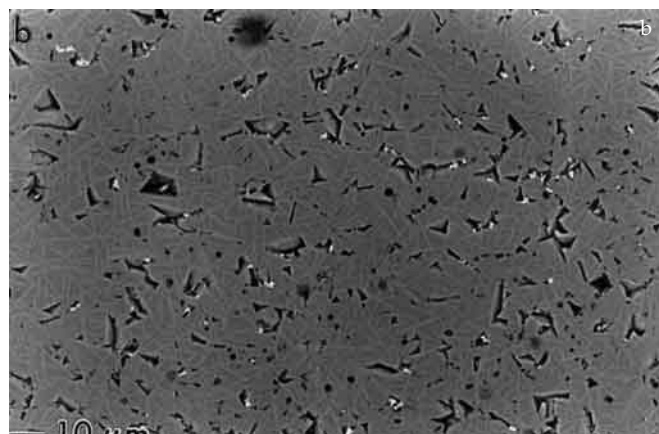
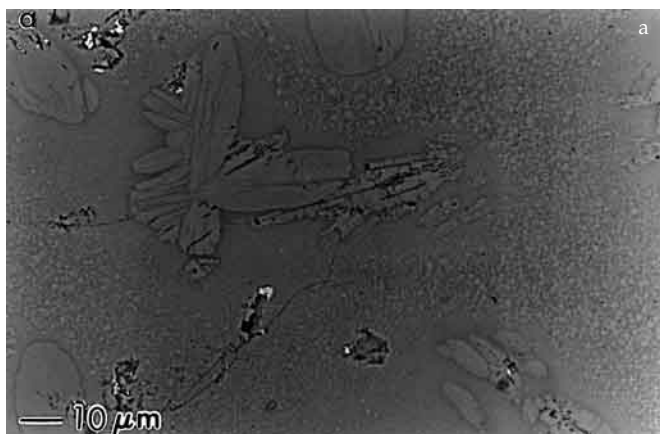


Fig. 2: Back-scattered electron micrographs of the quenched melt in samples A (a) and B (b). In the doped sample, Ti has only been detected in the light gray phase.

with the reduction of the grain size and the change in the viscosity of the melt that reduce the mobility of the bubbles.

3.2. Microstructure of the molten zone

At the end of the growth process, the molten zone was frozen in order to obtain additional information about the process that can induce these differences. Fig. 2 shows this molten zone in the case of samples A and B. As can be seen, two gray contrasts are distinguished in the micrographs of both samples. The phase distribution and the grain size in the doped sample are completely different compared to the undoped one. In the pure sample the dark gray phase forms a matrix at which the light gray one is dispersed in a pseudo-dendritic way. The higher the growth speed, the higher is the number of light gray phase particles because the growth conditions are far from equilibrium ones (18). The addition of Ti thus completely changes the microstructure. The grains of the light gray phase form a dense network in the matrix, increasing their number. In addition, the dimensions of these particles are one order of magnitude smaller than in the case of the undoped sample.

The composition of these phases has been determined using EDX and the results are presented in Table II. It is important to note that the Ti has only been detected in the light gray phase, where a concentration of 4.8 at% (Ti/(Cu+Ti)) has been found. By contrast, the matrix phase (dark gray) is a Ti free phase or the amount of Ti on it is lower than the minimum that can be detected with EDX.

3.3. Microstructure of the textured samples

Fig. 3 shows the interface of the molten zone with the textured region in the as-grown sample A. In the textured sample, three contrasts are distinguished. The primary solidification phase is the Bi-free oxide $\text{Sr}_{1-x}\text{Ca}_x\text{CuO}_2$ (black contrast in the micrographs). This phase nucleates in the light gray phase of the molten zone. In addition, also two gray contrasts are present. A light gray phase, which grows from the light gray phase of the molten zone, is also present in the textured region. As can be observed in Table II the amount of Ca in this phase is very low and has been assigned to intergrowths of the Bi-2201 and the Bi-2212 phases. This is the main phase in the as-grown samples. The dark gray phase, which fills the holes between the previous grains in

TABLE II. EDX ELEMENTAL ANALYSIS OF THE DIFFERENT PHASES THAT ARE PRESENT IN THE UNDOPED AND DOPED SAMPLES. THE MAIN PHASE IS PRESENTED IN BOLD. IN ADDITION, SMALL GRAINS OF CaO ARE PRESENT IN THE AS GROWN AND IN THE ANNEALED TEXTURED SAMPLES. FOR THE DOPED SAMPLES, THE PHASES IN WHICH THE AMOUNT OF Ti IS HIGH ENOUGH TO BE DETECTED BY EDX HAS BEEN UNDERLINED. IN THE AS-GROWN DOPED SAMPLES, TWO LIGHT GRAY PHASES ARE PRESENT, THE SECOND ONE CORRESPONDS TO GRAINS CLOSE TO THE $\text{Sr}_{1-x}\text{Ca}_x\text{CuO}_2$ ONES WHERE A HIGHER AMOUNT OF Ti HAS BEEN DETECTED.

	Undoped sample Bi:Sr:Ca:Cu	Doped sample Bi:Sr:Ca:Cu:Ti	Chemical phase
Frozen melt			
Dark gray	39:17:12:31	35:17:15:33:0	
Light gray	43:18:12:27	41:21:10:26:1.3	
As-grown samples			
Black	0:27:24:57	0:20:25:55:0	$\text{Sr}_{1-x}\text{Ca}_x\text{CuO}_2$
Dark gray	34:12:14:39	35:14:16:34:0	2212
Light gray	49:19:6:26	45:22:7:24:1.0	2201+2201
Light gray*		47:21:6:22:2.8	2201+2212
Annealed samples			
Black1	0:4:60:36	0:4:61:35:0	Ca_2CuO_3
Black2	0:20:24:56	0:23:20:55:0	$\text{Sr}_{1-x}\text{Ca}_x\text{CuO}_2$
Dark gray	35:19:14:32	34:20:13:32:0	2212
Light gray	48:21:6:24	47:19:8:25:0.9	2201+2212

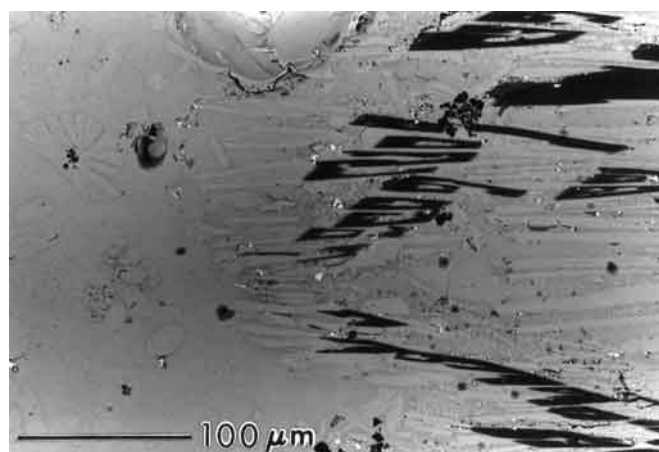


Fig. 3: Back-scattered electron micrograph of the interface between the molten zone (left) and the textured region (right) in sample A.

the textured sample, does not show any textured structure. Its composition coincides with the composition of the main phase in the annealed samples and, in consequence, has been correlated with the Bi-2212 phase.

In the case of the doped samples, the same phases are present and the mechanisms that control the grain growth are similar. The previously mentioned differences in the molten zone are responsible for the reduction of the grain sizes. In addition, as can be observed in Fig. 4, the texture of the doped samples is worse. In the undoped case (Fig. 4a) it is seen that the Bi-2201+Bi-2212 grains mainly follow the orientation of the $\text{Sr}_{1-x}\text{Ca}_x\text{CuO}_2$ ones. Besides, the sample shows a microstructure in which the small angle grain boundaries, that are responsible for the high intergranular pinning (3), can be easily observed. In the doped samples, the image is completely different (Fig. 4b). The $\text{Sr}_{1-x}\text{Ca}_x\text{CuO}_2$ grains induce some texture around themselves but this is not enough to orient the rest of the Bi-containing grains. In consequence, the orientation of these grains in the doped samples is much poorer than in the undoped ones. The small black grains that are present in both samples correspond to CaO grains. They remain after annealing.

As in the molten zone, Ti could only be detected, with EDX, in the light gray textured phase. The amount of Ti is similar to that observed in the light gray phase of the molten zone, namely 5.1 at% of Ti. As can be observed in Fig. 5, each of the $\text{Sr}_{1-x}\text{Ca}_x\text{CuO}_2$ grains is surrounded by a grain of the light gray phase. In these grains the amount of Ti can reach a 10 at% due to the migration of other ions to the non-superconducting grains. For this reason, two compositions of the light gray phase are present in Table II. In the other phases that are present, the amount of Ti is lower than could be detected with EDX.

After annealing, the dark gray phase becomes the main one and has been assigned to the Bi-2212 phase, in accordance to the electrical characterization. Some grains of the $\text{Sr}_{1-x}\text{Ca}_x\text{CuO}_2$ phase are also present, in particular in the border of the sample. Another non-superconducting phase appears after annealing, with a composition Ca_2CuO_3 . The Ti, in the doped samples, only can be detected with EDX in the light gray phase grains (less than 5 at% of Ti). However, it is likely that Ti is also dissolved in the superconducting grains because the critical temperature of the doped samples is some degrees lower than in the undoped ones, see below. This is a fact similar to the behavior observed in single crystals (9).

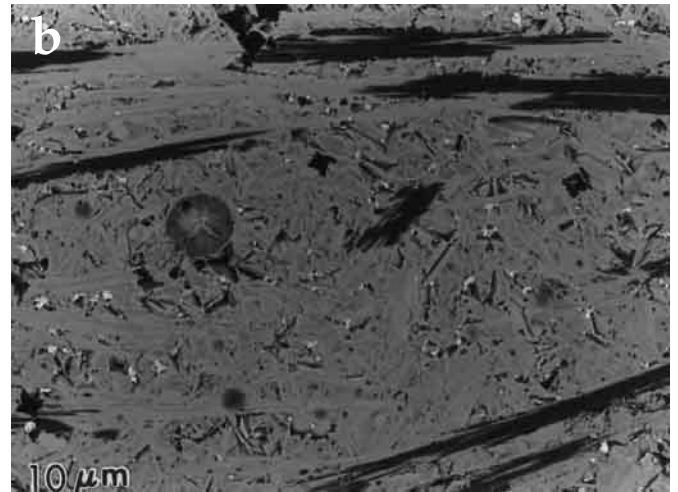
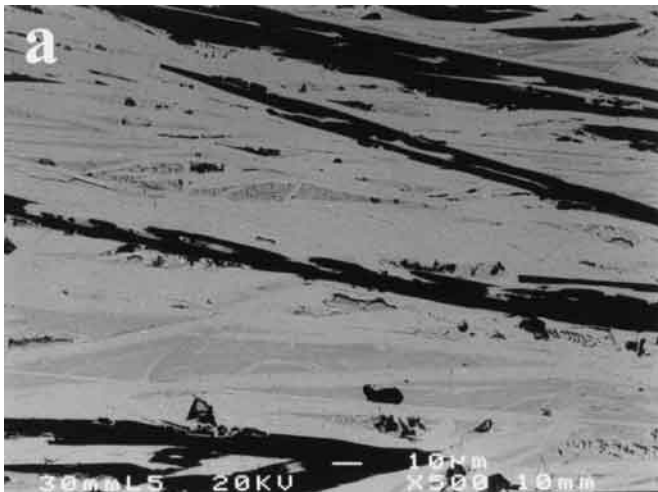


Fig. 4: Back-scattered electron micrographs of a longitudinal cross-section in the center of the samples A (a) and B (b) before annealing.

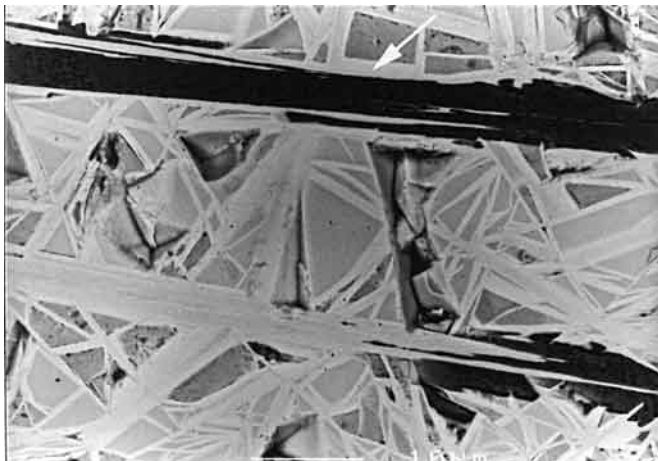


Fig. 5: Detail of a longitudinal cross-section of sample B showing with an arrow the grains where a higher amount of Ti has been detected with EDX.

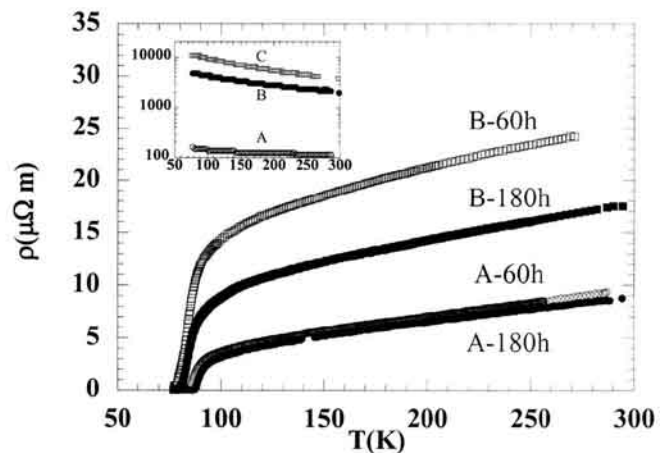


Fig. 6: Evolution of the resistivity with temperature in samples A (circles) and B (squares) after an annealing of 60 h (open symbols) and 180 h (closed symbols). In the inset, the temperature dependence of the resistivity in the three as-grown samples is depicted.

4. SUPERCONDUCTING PROPERTIES

All the above effects of the Ti addition on the microstructure are also reflected in the superconducting properties. The inset of Fig. 6 shows the temperature dependence of the normal resistivity in the as-grown rods. All the samples show a semiconductor-like behavior in accordance to the majority of the Bi-2201 phase in their composition. As can be seen and as is presented in Table III, the resistivity value is one order of magnitude higher in the doped samples. This is in agreement with the previously discussed differences in the microstructure because it reflects the higher amount of the Bi-2201 phase and the worse quality of the intergranular junctions. In undoped samples it is established that if the growth speed is reduced, the solidification process occurs close to equilibrium conditions and the amount of Bi-2212 phase increases, reducing the ratio $\rho(77\text{K})/\rho(300\text{K})$. Even at very low growth speeds, the behavior can change to metallic. Table III shows that this ratio is higher in the doped samples.

As is well established in this textured material (15) after a short annealing the Bi-2212 phase becomes predominant and, in consequence, the temperature dependence of the resistivity changes to the usual metallic behavior associated with this phase. In well-textured samples, as in this work sample A, the main changes due to annealing take place in less than 60 h. They are due to diffusion processes, which adjust the composition without nucleation of new grains, and in consequence, without an improvement of the texture (15, 19). In worse textured samples, in addition to diffusion mechanisms, there is nucleation of new grains that helps to improve the texture during annealing (19). Fig. 6 shows the influence of the annealing in the case of sample A and B. An idea of the behavior of the sample C can be obtained from the data presented in Table III. The differences between the data after 60 h of annealing or after 180 h are not very important in the case of the undoped sample, showing that the main changes in the samples have taken place in the initial annealing, as it was expected. By contrast, in the doped samples an improvement in the following annealing can also be detected. This fact indicates that the evolution of the microstructure in the doped samples requires longer annealing because the undoped sample microstructure was closer to equilibrium conditions.

In all the cases, the data above 200 K have been fitted to a linear dependence, $\rho(T) = \rho_0 + \alpha T$. The residual resistivity, ρ_0 , decreases as an indication of the improvement of the intergranular junctions during annealing. A similar behavior is observed in the slope of the curve, α .

After 180 h of annealing, the critical temperature defined as the temperature at which the resistivity becomes negligible, T_{onset} , is around 6 K lower in the doped samples. This reduction is in accordance with the results obtained from ac-susceptibility (Fig. 7), where a similar reduction has been observed in the value of T_{diam} . These data are in agreement with the effects observed in single-crystals doped with Ti or other 3d elements (8). This reduction of the critical temperature, in combination with the increase of the width of the superconducting transition (6.5 K in sample A and 14 K in sample B), the temperatures at which the peak of the out-of-phase component of χ_{ac} appears (88 K in sample A and 68 K in sample B) and the texture degradation explain the poor critical currents of the doped samples in the high temperature range (see Table III). These detrimental effects of Ti-addition

TABLE III. SUPERCONDUCTING PARAMETERS OF THE DIFFERENT SAMPLES OBTAINED FROM TRANSPORT AND AC MAGNETIC SUSCEPTIBILITY MEASUREMENTS IN AS-GROWN SAMPLES AND AFTER ANNEALINGS OF 60 AND 180 H AT 843°C. THE RESISTIVITY DATA OF THE ANNEALED SAMPLES FOR $T > 200$ K HAVE BEEN FITTED TO A LINEAR TEMPERATURE DEPENDENCE $\rho(T) = \rho_0 + \alpha T$.

	Sample A	Sample B	Sample C
Diameter (mm)	1.40	1.45	1.40
As-grown			
$\rho(300\text{K})$ ($\mu\Omega$ m)	120	2100	3800
$\rho(77\text{K})/\rho(300\text{K})$	1.5	2.5	2.9
Annealed 60 h			
ρ_0 ($\mu\Omega$ m)	1.9	10.4	12.8
α ($\mu\Omega$ m / K)	0.026	0.040	0.042
T_{onset} (K)	84.7	<77	<77
T_{diam} (K)	89	80	80
$T_{\text{max}\chi}$ (K)	88	68	67
Annealed 180 h			
ρ_0 ($\mu\Omega$ m)	1.8	5.2	7.3
α ($\mu\Omega$ m / K)	0.024	0.029	0.034
T_{onset} (K)	87.0	80.3	81.3
$I_c(77\text{K})$ (A)	48.2	1.2	<1
$I_c(65\text{K})$ (A)	150	15.5	1

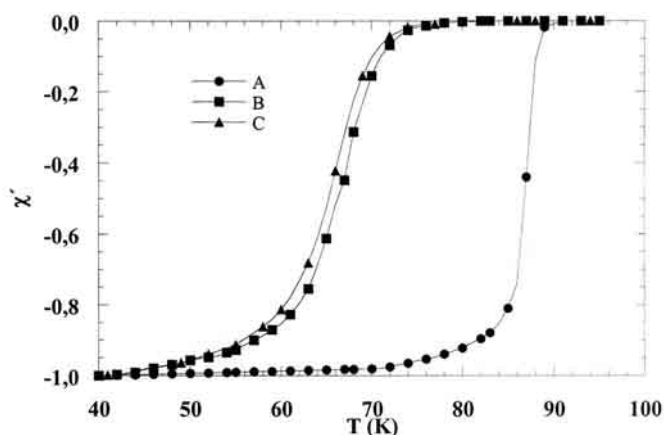


Fig. 7: Temperature dependence of the ac susceptibility in the samples after an annealing of 60 h. The ac field (0.2 Oe of amplitude and 171 Hz of frequency) has been applied parallel to the rod axis.

on superconducting properties have also been observed in Bi-2212 and Bi-2223 ceramics (20) and thick films (21).

In order to reduce the effects associated with the reduction of T_c and to obtain information about pinning at low temperatures, magnetization hysteresis loops were measured at 5 K, with the magnetic field applied parallel and perpendicular to the rod axis. The width of this hysteresis loops is about 10 times higher in sample A than in B. Due to the high differences in the microstructure it is difficult to determine with is the length scale of the currents and for this reason we cannot compare estimates of the critical current density. For this reason Fig. 8 shows the evolution of the width of the hysteresis loops scaled to the value of $\Delta M(0.5\text{T})$ with the field applied perpendicular to the rod axis. First we can notice that the width decays faster with magnetic field in the doped samples indicating a lower pinning. A second point to remark is the differences between the width measured with the field applied parallel and perpendicular to the rod axis. In the case of the doped sample the ratio between the width of both

loops is around 0.5 what is the expected value considering demagnetization effects. In the case of the undoped sample, the ratio reduces to 0.25. This result indicates that in this sample, the critical current is anisotropic, lower in the azimuthal direction than in the longitudinal one. The doped sample shows a more isotropic behavior as a consequence of its microstructure in which the alignment of the grains is poorer.

This behavior is in contrast to what it is observed in doped single crystals, where the critical current density at 15 K was about 4 times higher (8), and the irreversibility line was shifted to higher fields and temperatures as compared to undoped single crystals.

5. CONCLUSIONS

Ti has been introduced in the precursor of LFZ Bi-2212 textured samples with the aim of studying the possible benefits for the critical current density as might be expected from results on Ti-doped single crystals (8). It was found that Ti acts as a strong nucleation factor inducing great changes in the microstructure of the samples. The grain dimensions of the doped samples are one order of magnitude smaller, inducing a great misorientation in the sample texture. In addition, the critical temperature of the doped samples is about 8 K lower than in the undoped ones. This fact and the worse texture of the doped samples, give rise to lower critical currents using the same growth conditions. At low temperatures, the performance of the doped samples, in particular the field dependence of the critical current density is also poorer. Ti strongly deteriorates the microstructure of these LFZ textured Bi-2212 rods because Ti addition destroys the low angle grain boundaries that were responsible of the high critical currents of the undoped material. The experiments that have been presented in this paper have been performed on samples that have been grown at relatively high growth rates. As Ti induces pinning centers in single-crystals, a similar study on samples grown at low growth rates could be interesting.

ACKNOWLEDGEMENTS

Authors are indebted to the Spanish CICYT and the European Commission (project 2FD97-0546-C04-01) and Dutch FOM for the financial support of this research.

REFERENCES

1. P.F. Herrmann. "Current leads", pp 801-843, in Handbook of Applied Superconductivity (Ed. by B. Seeber, IOP), Vol I (1998).
2. L.A. Angurel, G.F de la Fuente, A. Badía, A. Larrea, J.C. Díez, J.I. Peña, E. Martínez, R. Navarro. "Textured BSCCO superconductors obtained via laser induced directional solidification", pp. 1-31, in Studies of High Temperature Superconductors (Ed. By A.V. Narlikar, Nova Science, New York), Vol. 21 (1997).
3. M. Mora, J. Fernández, L.A. Angurel, R. Navarro. "Pinning by planar high Jc defects and self field limited currents of textured Bi-2212 thin rods". Physica C 312 [1-2], 136-148 (1999).
4. E. Martínez. "Imanación y corrientes críticas en fibras gruesas BSCCO: texturado y anclaje de flujo". PhD Thesis, University of Zaragoza, Spain (1997)
5. E. Martínez, L.A. Angurel, J.C. Díez, F. Lera, R. Navarro. "Magnetic relaxation of highly textured Bi₂Sr₂CaCu₂O_{8+δ} polycrystalline fibres". Physica C 271 [1-2], 133-146 (1996).

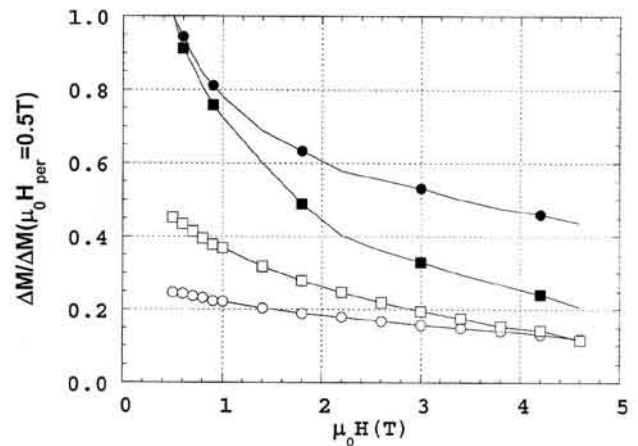


Fig. 8: Evolution of the width of the hysteresis loops (normalized to the value obtained with a field of 0.5T applied perpendicular to the rod axis), at 5 K in sample A (circles) and B (squares). Open symbols have been used to present the data obtained for fields applied perpendicular to the rod axis and closed ones for fields applied parallel to the rod axis.

6. V. Hardy, J. Provost, D. Groult, M. Hervieu, B. Raveau, S. Durcok, E. Pollert, J.C. Frison, J.P. Chaminade, M. Pouchard. "Strong shift of the irreversibility line in bismuth and thallium based 2212 HTSC single crystals irradiated by 6.0 GeV Pb ions". Physica C 191 [1-2], 85-96 (1992).
7. H.W. Weber, G.W. Crabtree. "Neutron irradiation effects in high Tc single crystals", pp. 37-79, in Studies of High Temperature Superconductors, (Ed. By A.V. Narlikar, Nova Science, New York), Vol. 9 (1991).
8. J.H. Cho, H.F. Safar, M.P. Maley, J.O. Willis, J.Y. Coulter, D.G. Steel, K.E. Gray. "Effects of unidirectional and isotropic columnar defects in Bi₂Sr₂CaCu₂O₈ single crystals". Physica C 302, 113-118 (1998).
9. T.W. Li, R.J. Drost, P.H. Kes, C. Traeholt, H.W. Zandbergen, N.T. Hien, A.A. Menovsky, J.J.M. Franse. "Enhanced flux pinning in Bi-2212 single crystals by planar defects introduced via Ti-substitution". Physica C 274 [3-4], 197-203 (1997).
10. R.J. Drost, T.W. Li, P.H. Kes, R. Surdeanu, R.J. Wijngaarden, M. Konczykowski. "Bulk pinning by planar defects in Ti-doped Bi-2212 single crystals". Physica C 282-287, 2241-2242 (1997)
11. H. Horvat, X.L. Wang, S.X. Dou. "Vortex pinning in heavily Pb-doped Bi2212 crystals". Physica C 324 [3-4], 211-219 (1999).
12. A.L. Crossley, Y.H. Li, A.D. Caplin, J.L. MacManus-Driscoll. "The effect of low oxygen partial pressure and high Pb-doping on Bi-2212 phase formation and flux pinning". Physica C 314 [1-2], 12-18 (1999).
13. P.E. Kazin, V.V. Poltavets, O.N. Poltavets, A.A. Kovalevsky, Yu.D. Tretyakov, M. Jansen. "Formation of Bi-2212 phase and phase assemblage in Ga-doped BSCCO system". Physica C 324 [1], 30-38 (1999).
14. L.A. Angurel, J.C. Díez, E. Martínez, J.I. Peña, G.F. de la Fuente, R. Navarro. "Growth rate effects on thin Bi₂Sr₂CaCu₂O_{8+δ} textured rods". Physica C 302 [1], 39-50 (1998).
15. M. Mora, E. Martínez, J.C. Díez, L.A. Angurel, G.F. de la Fuente. "Phase growth and microstructure modifications induced by annealing in highly textured superconducting Bi-2212 thin rods". Journal of Material Research 15 [3], 614-620 (2000).
16. S.W. Poole, J.E. Franklin. "High-strength structural and high-strength low-alloy steels", pp. 403-420, in Metals Handbook, 9th Edition, Vol 1, Ed. by American Society for Metals, Ohio (1978).
17. Y.M. Chiang, D.P. Birnie III, W.D. Kingery. Physical Ceramics: Principles for Ceramic Science and Engineering. John Wiley & Sons, Inc, 1997.
18. W.G. Pfann, in Zone Melting, (2nd ed.) John Wiley & Sons, New York (1966).
19. E. Martínez, L.A. Angurel, J.C. Díez, A. Larrea, M. Aguiló, R. Navarro. "Grain texture and bulk magnetic anisotropy correlation in polycrystalline Bi₂Sr₂CaCu₂O_{8+δ} thin rods". Physica C, 333 [1-3], 93-103 (2000).
20. N.A. Hamid, R. Abd-Shukur. "Effects of TiO₂ addition on the superconducting properties of Bi-Sr-Ca-Cu-O system". Journal of Materials Science 35, 2325-2329 (2000).
21. H.K. Barik, S. Bhattacharya, S. Chatterjee, P.K. Pal, B.K. Chaudhuri. "Effect of Ti doping on the transport properties of thick films of (Bi, Pb)-Sr-Ca-(Cu, Ti)-O -type glass-ceramic superconductors". Philosophical Magazine B, 79 [8], 1161-1173 (1999).

Recibido: 19.12.01

Aceptado: 18.01.03